Biophysical Journal, Volume 99

Supporting Material

Anisotropic Elastic Network Modelling of entire Microtubules

Marco A. Deriu, Monica Soncini, Mario Orsi, Mishal Patel, Jonathan W. Essex, Franco M. Montevecchi, and Alberto Redaelli

SUPPORTING MATERIAL 1

Refining tubulin dimer atomic structure 1TUB

The αβ-tubulin atomic structure was obtained with a resolution of 3.7 Å by Nogales and coworkers (1) using electron crystallography; the structure is available on the RCSB Protein Data Bank (1TUB code).
Several initial refinements of the tubulin atomic structure were carried out to obtain a molecular model representative of the tubulin dimer under physiological conditions (2-3).
The 1TUB structure lacks several residues, i.e., 10 for α-tubulin and 18 for β-tubulin, in the C-terminals, due to a large variation among monomer isotypes, which made this part of the structure difficult to identify. The Taxol molecule, needed for the protein crystallization, was removed from the 1TUB structure, since Taxol is not present under physiological conditions. A Mg^{2+} ion, which conversely is present under physiological conditions (2), was inserted setting its position according to the 1JFF (1JFF.pdb file) tubulin structure (4).
Hence, the refined tubulin dimer atomic structure (FIGURE 1) contained atomic coordinates for: α-tubulin monomer, guanosine-5'-triphophate (GTP), Mg^{2+} ion, β-tubulin monomer and guanosine-5'-diphosphate (GDP).

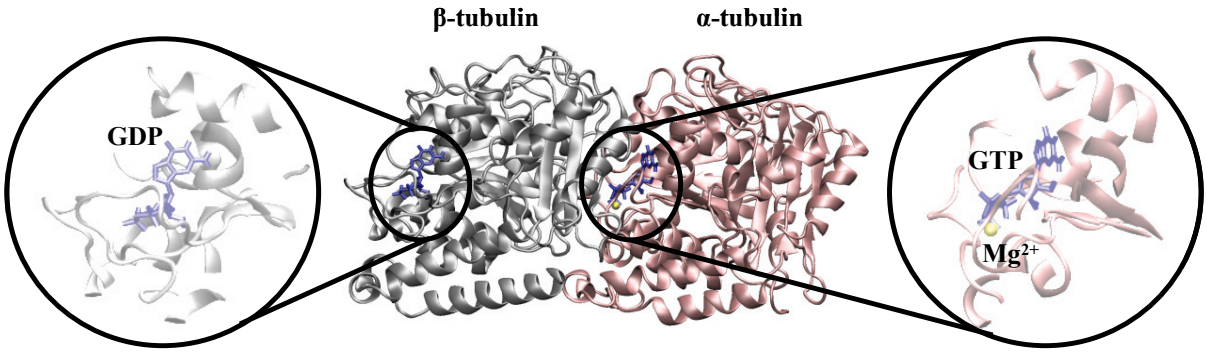

FIGURE 1 The refined tubulin dimer for building the 12-tubulin cluster. Guanosine-5'-triphophate (GTP), Mg^{2+} ion, and guanosine-5'-diphosphate (GDP) are highlighted in the zoomed inserts of the figure. GTP and GDP nucleotides are represented by sticks, while the rest of the protein is represented by ribbon visualization.

Remodelling the H1-B2 loop

To build the tubulin-sheets consisting of 12 tubulin monomers, the 1TUB atomic structure has been used as the initial configuration of the tubulin dimer. Each dimer position in the MT lattice can be determined based on the literature information about the position assumed by the tubulin dimers in the MT lattice structure (1, 4-10). To obtain a correct positioning of the tubulin monomers in the MT lattice structure, and thus a proper curved conformation of the tubulin-sheets (standard and seam sheets), the tubulin dimer (1TUB.pdb) has been docked onto a 13-protofilament, 3-start-helix MT model (9).
However, the 1TUB crystallographic structure just extracted from the Protein Data Bank, is not a suitable structure to be inserted onto the MT lattice, even if it contains a complete description of

the tubulin dimer. In particular, the 1TUB α-monomers rigidly positioned in the MT lattice showed some interlocking loops between adjacent monomers in the lateral surface (FIGURE 2). The interlocking loops are the M-loop and the H1-B2 loop.

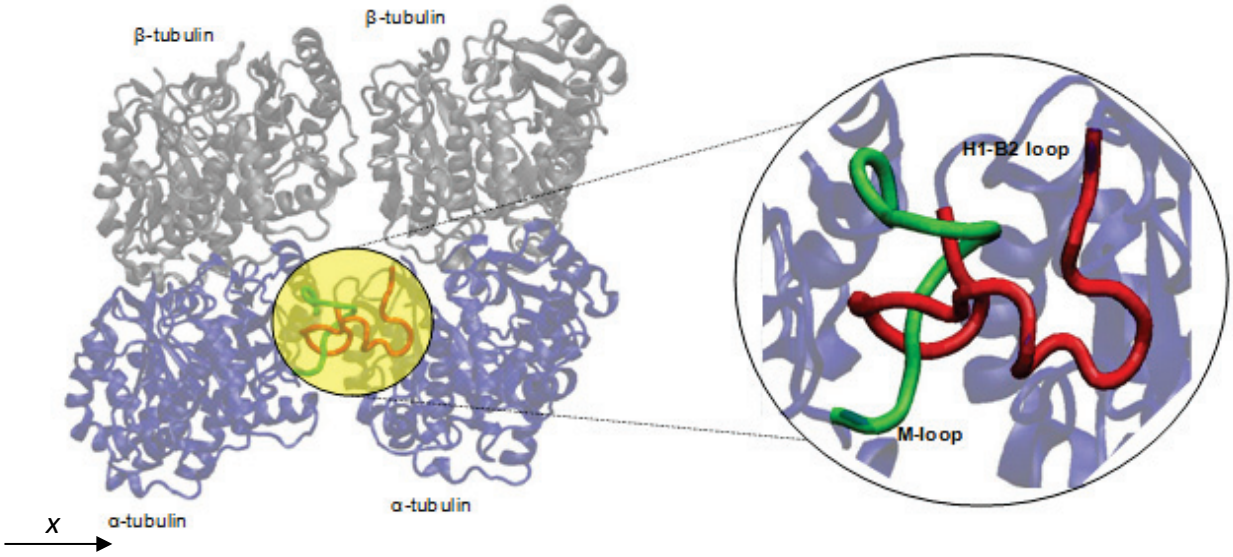

FIGURE 2 Interlocking α-tubulins. By positioning the 1TUB structure in the MT lattice (9), the H1-B2 loop (red with tube mode visualization) of an α-monomer and the M-loop (green with tube mode visualization) in the adjacent monomer result locked in a non-physiological way. The picture in the zoom on the right is slightly rotated around the x axis with respect to the main picture on the left in order to better show the ring-like connection.

The reason for this kind of connection, which is supposed to be not physiologically possible, lies probably in the wrong residue conformation in terms of atom positions assigned by the crystallographic analysis (1). In fact, the 1TUB structure has been determined by means of electron crystallography with low resolution (0.37 nm) and the model has been built in a rough density map without refinement (1). We identified the H1-B2 loop (residues 24-64 in the α-monomer) as responsible for the interlocking connection occurring at the lateral surface. This sequence of residues, close to the N-terminal, is entirely missing in the refined structure of the tubulin dimer, coded 1JFF (4). In fact, this aminoacid segment represents the poorest density area for both α- and β-monomer (4). In the case of the α-monomer the refinement procedure "did not result in an improvement of the density, but rather a disappearance of part of it" (4). Given that the interaction between the M-loop and the H1-B2 loop represents the most important interaction surface for the lateral contacts between α-monomers, the entire α-tubulin H1-B2 loop was remodeled by using the software MODELLER (11-12) combined with a simulated annealing procedure. MODELLER is a computational code used for homology or comparative modeling of three-dimensional structures of proteins.

Owing to the high sequence homology between α- and β- monomers, the H1-B2 loop in the β-tubulin (accurately described in both 1TUB and 1JFF atomic structures) was used as template for arranging the starting tertiary structure of the H1-B2 loop in the α-tubulin atomic structure. By

means of specific tools available in MODELLER the primary sequence of the α-tubulin H1-B2 loop was spread on the tertiary structure over the same loop in the β-tubulin.
To find a suitable tertiary structure as template for the α-tubulin H1-B2 loop, the loop sequence was aligned with several other protein primary sequences using FASTA (13), an heuristic software able to find global sequence homologies among proteins by searching in a database of protein primary sequences.
In FIGURE 3 the FASTA alignment between the primary sequences of the α-tubulin and β-tubulin H1-B2 loops is shown, as the alignment with highest degree of similarity among all the structures contained in the European Bioinformatic Database (EBI) database (www.ebi.ac.uk).

```
>>PDB:1TUB_B mol:protein length:427  TUBULIN                (427 aa)
 initn:  92 init1:  53 opt:  86  Z-score: 132.7  bits: 30.2 E():  1.7
Smith-Waterman score: 86; 34.2% identity (78.9% similar) in 38 aa overlap (4-41:27-62)


Sequen                          YCLEHGIQPDGQMPSDKTIGGGDDSFNTFFSETGAGK
                                   ::::.: :.. .:. .    . .:....:....:
PDB:1T MREIVHIQAGQCGNQIGAKFWEVISDEHGIDPTGSYHGDSDLQ--LERINVYYNEAAGNK
               10        20        30        40          50

        40
Sequen HVPR
       .:::
PDB:1T YVPRAILVDLEPGTMDSVRSGPFGQIFRPDNFVFGQSGAGNNWAKGHYTEGAELVDSVLD
       60        70        80        90       100       110
```

FIGURE 3 Alignment of the α-monomer H1-B2 loop sequence on the β-monomer sequence (residues from 24 to 62). The sequence of the H1-B2 loop of the α-monomer consists of 41 residues, highlighted in yellow. The identity resulted 34.2%, while the similarity is equal to 78.9%.

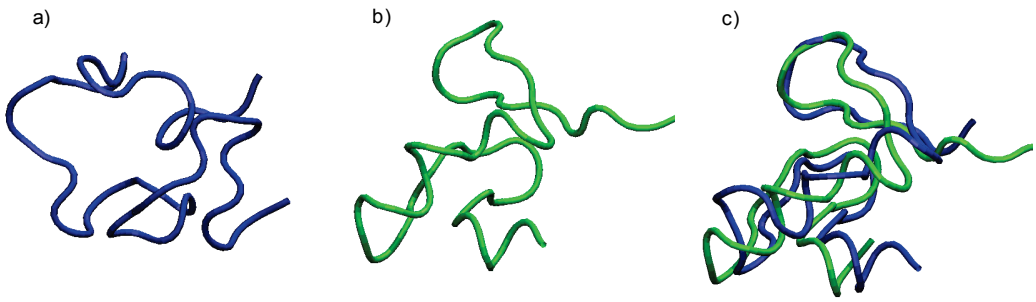

FIGURE 4 Remodeling of the original H1-B2 loop of the α-monomer starting from 1TUB.pdb file (a) by spreading it on the same loop found in the β-monomer (b), by means of MODELLER software. The final conformation after the spreading is shown in panel (c), where the H1-B2 loop from the β-monomer is colored in green and the remodeled H1-B2 α-monomer loop is represented in blue.

The spreading procedure here used, just gave a new loop conformation close to the H1-B2 loop of the β-monomer (FIGURE 4). Since the correct conformation of the loop was completely unknown, a Simulated Annealing (SA) MD procedure was carried out in order to obtain and select a reasonable conformation of the H1-B2 loop.
In this particular case, the SA approach has been used to generate several random conformations of the H1-B2 loop. The temperature coupling was applied during the MD simulation by means of an external thermal bath and cyclically changing its temperature from 300 K to 500 K (heating

phase), from 500 K to 100 K (cooling phase) and then to 300 K (equilibration phase) following the scheme shown in FIGURE 5. The SA MD simulation was carried out for 6 ns performing 3 cycles of heating-cooling-equilibration.

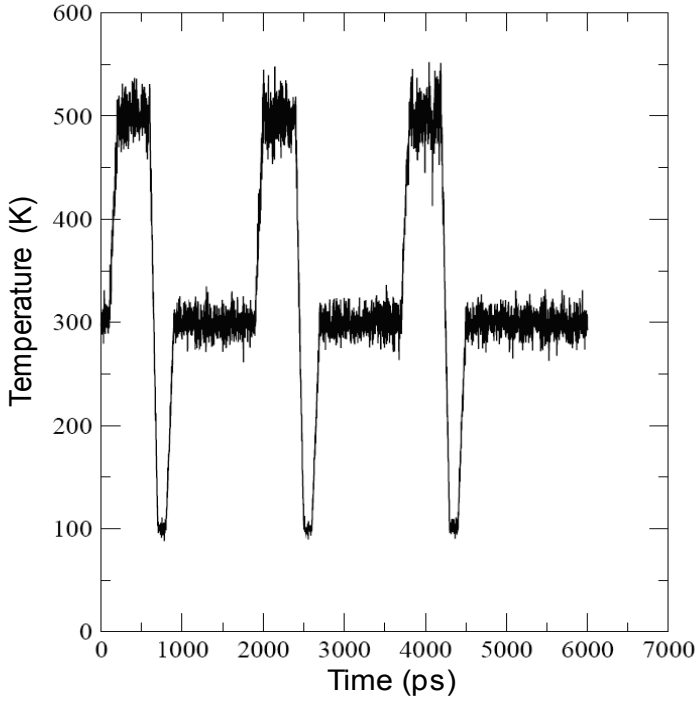

FIGURE 5 Simulated annealing procedure: periodic cycles of melting and cooling were applied in order to generate conformations far from the starting local minimum for the H1-B2 loop of the α-monomer.

Since the SA procedure was aimed at generating random conformational changes of the H1-B2 loop, very high non-physiological temperatures (500 K) were used in the annealing procedure, because the energy barriers can be more easily overcome at such temperatures than at 300 K.
The molecular system for the SA procedure consisted of 4 tubulin monomers (in order to save computational time only two dimers were simulated surrounding the loop) with the loop in the center of the system as shown in FIGURE 2, in order to create a physiological boundary condition for the loop. The simulation was performed in explicitly modeled water (water is not shown in FIGURE 2). Moreover the entire system beside the loop was kept frozen during the SA MD simulation since the approach was aimed at finding a suitable conformation just for the loop, while the atomic coordinates of rest of the dimer were already precisely given (1) and refined (4).
Six hundred possible conformations were extracted from the SA MD simulation. Among them, the choice of the best structure was carried out on the basis of a quantitative evaluation of the distance between atoms in the H1-B2 loop and the M-loop.

Refinement of the H1-B2 loop

The conformations of the H1-B2 loop were extracted from the MD trajectory by sampling every 10 ps. Owing to the high temperature peaks occurring during the SA MD simulation, the extracted conformations strongly differ in shape and distance from the M-loop (FIGURE 6).

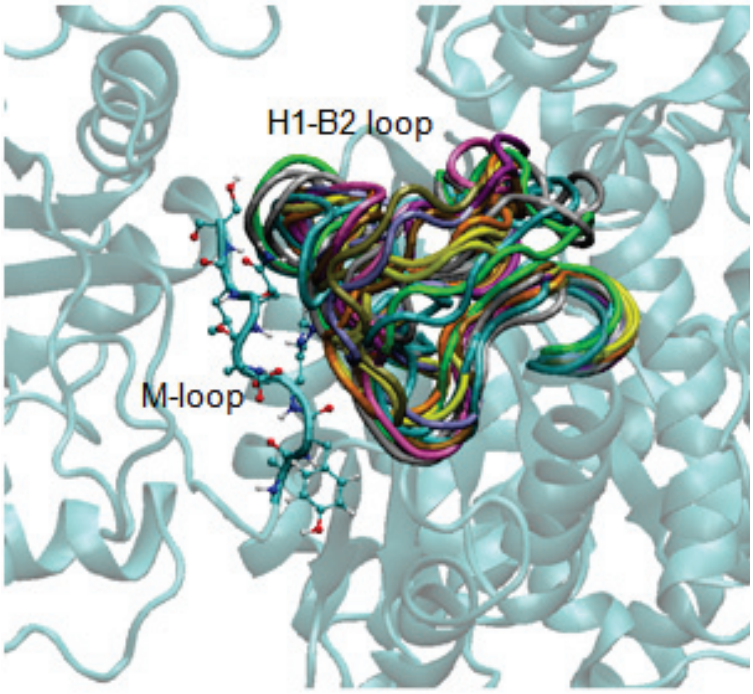

FIGURE 6 Different conformations (12 configurations) of the H1-B2 loop by sampling the SA MD trajectory every 500 ps. The H1-B2 loop conformations are shown in different colours with tube mode visualization, while the M-loop is shown with CPK mode visualization for the lateral chain atoms in combination with tube mode visualization for the backbone**. The** rest of the tubulin monomers are represented by ribbon visualization.

To select the best configuration for the H1-B2 loop, the minimum distance, D_{min}, between the residues belonging to the M-loop and the residues belonging to the H1-B2 loop, was compared. In FIGURE 7, the D_{min} *vs.* the residue number of the H1-B2 loop is plotted. In particular, each point of the plot represents the minimum distance between the residue Center of Mass (CM) in the H1-B2 loop (plotted in the x-axis) and its closest residue CM in the M-loop, which was kept frozen during the SA MD simulation.

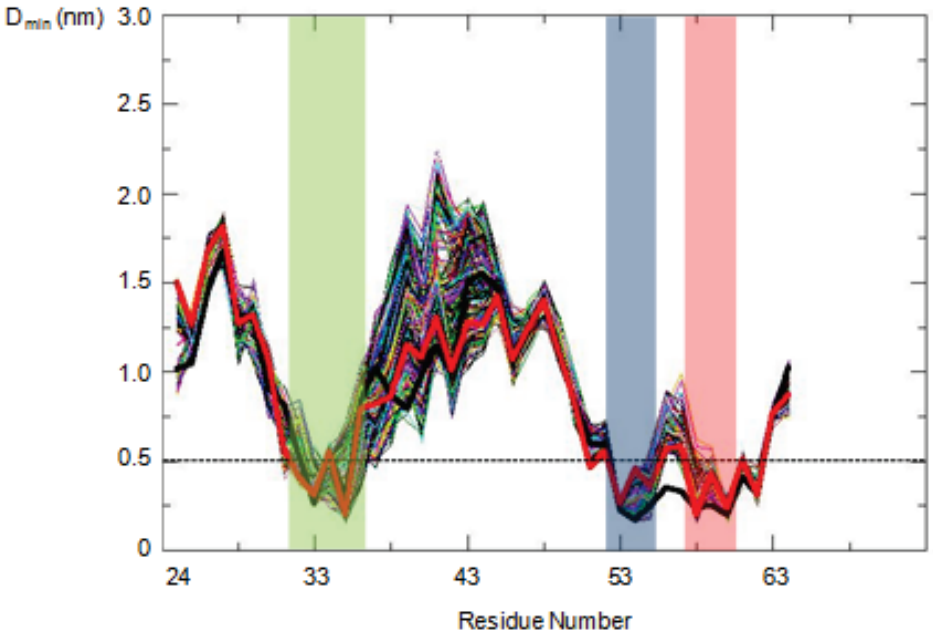

FIGURE 7 Minimum distance, D_{min}, *vs.* residue number of the H1-B2 loop. Each point of the plot represents the minimum distance, between the residue CM in the H1-B2 loop and its closest residue CM in the M-loop. The black thick curve indicates the D_{min} in the starting configuration while the red thick curve represents the configuration selected minimizing the average D_{min} between the two loops. The dashed line parallel to the x-axis represents the threshold set to define a contact region between two interacting residues (0.5 nm). Based on this threshold, the three coloured regions in the plot identify three segments of the H1-B2 loop very close to the M-loop. The light green area identifies the residues 32-37, the light blue area identifies the residues 51-55 and the light red area identifies the residues 58-62.

The thick black curve represents the starting configuration (t=0), while the thick red curve represents the loop conformation minimizing the mean value of D_{min}, which was selected as starting H1-B2 loop conformation for the further analyses.
Defining a contact distance for all-atom interactions (under 0.5 nm), three main interaction regions in the H1-B2 loop were identified (FIGURE 7 and FIGURE 8 a):

- residue 32 to residue 37 (light green);
- residue 51 to residue 55 (light blue);
- residue 58 to residue 62 (light red);

Given that during the simulation, only the H1-B2 loop is allowed to move while the rest of the protein, and thus the M-loop, is kept frozen, D_{min} (FIGURE 7) represents also a qualitative measure of the residue fluctuations. A direct measure of the root mean square fluctuations (RMSF) for each residue (FIGURE 8b), shows a behaviour in agreement with the curves reported in FIGURE 7. In particular, the maximum RMSFs (FIGURE 8b, black curve) are found in loop regions not closely involved in the interaction between the H1-B2 loop and the M-loop. Notice that the fluctuations reduce considerably when considering only the last part of the SA MD simulation, where the temperature is constant (FIGURE 8b, red curve calculated from 5 to 6 ns). The reason is that in the last part of the simulation the system is coupled to a constant temperature of 300 K. Nevertheless,

the shape of the RMSF, does not change markedly meaning that the residues involved in the three main interaction regions (coloured areas in FIGURE 8b) are trapped by the interaction potential between the M-loop and H1-B2 loop, while the other regions can freely move under the effect of thermal motion.

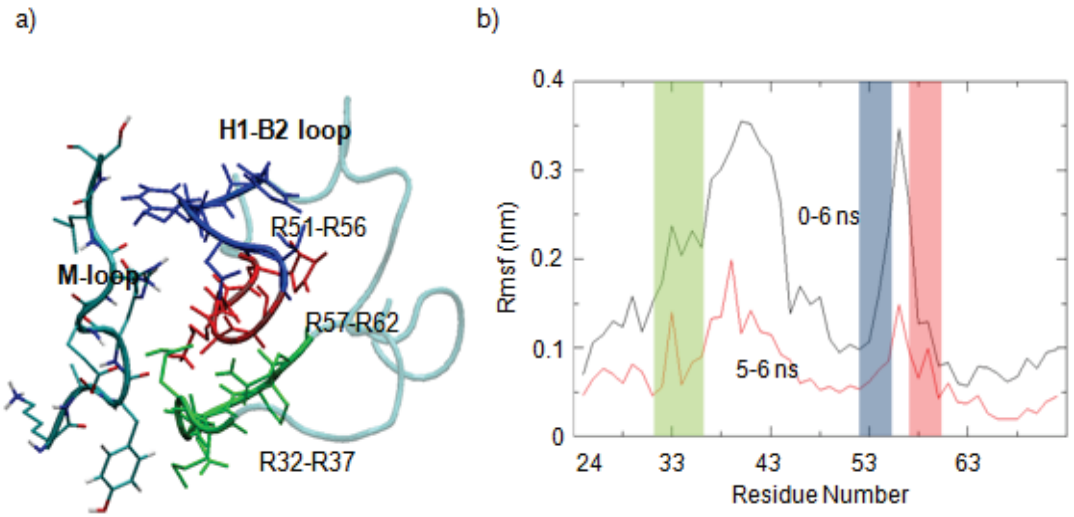

FIGURE 8 a) View of the chosen H1-B2 loop configuration. Three main region interacting with the M-loop were identified: residue 32 to residue 37 (light green), residue 51 to residue 55 (light blue), residue 58 to residue 62 (light red).-b) Root mean square fluctuations (RMSF) of H1-B2 residues calculated throughout the whole 6 ns simulation (blue curve) and in the last part of the SA simulation (from 5 to 6 ns, red curve). The three coloured regions in the plot identify the three main regions interacting with the M-loop.

Discussion

A first aspect to be considered is the the choice of the molecular structure, 1TUB (1), instead of other known atomic structures of the tubulin dimmer, 1JFF (4). The main difference between 1TUB and the refined 1JFF is related to the resolution of the density maps (3.5 Å for 1JFF and 3.7 Å for 1TUB), which is similar and very low in both cases. These crystallographic models have been solved in a Zinc-sheet structure, where protofilaments are assembled in an antiparallel manner and in a flat arrangement. In this way, the lateral surfaces of the tubulin monomers have a conformation which differs from that occurring in a curved MT lattice. In the 1JFF model the H1-B2 loop near the N-terminus is the poorest density area for both α- and β-tubulins. In particular, the H1-B2 loop is not solved for α-tubulin and residues 35-60 are lacking in the 1JFF model, together with some other residues at the terminals. In the 1TUB model the Mg^{2+} ion is missing. Anyway, when comparing the 1TUB and the refined 1JFF structures the authors themselves stated that "There are no major changes in the overall fold of tubulin with respect to the previous structure, testifying to the quality of the initial experimental phases." (4). So in the specific case of this work, there are no particular reasons to use 1JFF instead of 1TUB, because both require modifications and adjustments to obtain a proper dimer to fit in a MT wall-like curved structure.

Another important subject that has to be discussed is the remodeling strategy used to replace the H1-B2 loop in order to obtain a suitable structure to be docked into the MT lattice with proper contacts between the H1-B2 loop and M-loop of adjacent α-monomers. In previous studies several different strategies were adopted for this specific aim. In several investigations of the tubulin dimer alone, either 1TUB (2-3, 14-15) or 1JFF (16-17) were used without remodeling the H1-B2 loop, or just taking the atomic coordinates from 1TUB and adding them to the 1JFF structure, where residues 35-60 (i.e. the loop H1-B2) are not present (16). Some previous studies (17-19) dealt with the issue of reproducing the lateral interactions typical of the MT lattice; in those cases the H1-B2 loop of α-tubulin was rearranged. In particular Mitra and Sept (17) carried out MD simulations to investigate the role of Taxol in altering the dynamics of tubulin dimers and thus the stability of MTs. In that study, 1JFF structure was chosen and the H1-B2 loop of α-tubulin was modeled starting from the coordinates of H1-B2 loop in β-tubulin, since the two monomers are highly homologous. Then a minimization was carried out to correct the bonds, angles and torsions of the replaced residues. It is well known that a minimization strategy produces just a minor rearrangement of the structure, moving to the closest minimum (20). However, even if a significant homology between the two monomers exists, the conformational arrangement of the H1-B2 loop could be different in the α- and β-monomer owing to its flexibility, which makes it fluctuate under thermal motion. The remodeling procedure used in this work was aimed at sampling a possible conformation of the H1-B2 loop in the α-tubulin monomer by means of a method based on the evaluation of the H1-B2 loop interaction with the M-loop in the adjacent monomer. The SA MD procedure was aimed at obtaining greater sampling of the loop conformation with respect to what can be done by energy minimization procedures.

References

1. Nogales, E., S. G. Wolf, and K. H. Downing. 1998. Structure of the alpha beta tubulin dimer by electron crystallography. Nature 391:199-203.
2. Enemark, S., M. A. Deriu, M. Soncini, and A. Redaelli. 2008. Mechanical model of the tubulin dimer based on molecular dynamics simulations. J Biomech Eng 130:041008.
3. Deriu, M., S. Enemark, M. Soncini, F. Montevecchi, and A. Redaelli. 2007. Tubulin: from atomistic structure to supramolecular mechanical properties. Journal of Materials Science 42:8864-8872.
4. Lowe, J., H. Li, K. H. Downing, and E. Nogales. 2001. Refined structure of alpha beta-tubulin at 3.5 A resolution. J Mol Biol 313:1045-1057.
5. Downing, K. H., and E. Nogales. 1999. Crystallographic structure of tubulin: implications for dynamics and drug binding. Cell Struct Funct 24:269-275.
6. Downing, K. H., and E. Nogales. 1998. Tubulin structure: insights into microtubule properties and functions. Curr Opin Struct Biol 8:785-791.
7. Downing, K. H., and E. Nogales. 1998. New insights into microtubule structure and function from the atomic model of tubulin. Eur Biophys J 27:431-436.
8. Downing, K. H., and E. Nogales. 1998. Tubulin and microtubule structure. Curr Opin Cell Biol 10:16-22.
9. Li, H., D. J. DeRosier, W. V. Nicholson, E. Nogales, and K. H. Downing. 2002. Microtubule Structure at 8 Å Resolution. Structure 10:1317-1328.
10. Chretien, D., and R. H. Wade. 1991. New data on the microtubule surface lattice. Biol Cell 71:161-174.
11. Fiser, A., and A. Sali. 2003. ModLoop: automated modeling of loops in protein structures. Bioinformatics 19:2500-2501.
12. Sali, A., L. Potterton, F. Yuan, H. van Vlijmen, and M. Karplus. 1995. Evaluation of comparative protein modeling by MODELLER. Proteins 23:318-326.
13. Pearson, W. R. 1990. Rapid and sensitive sequence comparison with FASTP and FASTA. Methods Enzymol 183:63-98.
14. Soncini, M., E. Votta, I. Aprodu, S. Enemark, A. Redaelli, M. A. Deriu, and F. M. Montevecchi. 2009. MICROTUBULE-KINESIN MECHANICS BY MOLECULAR MODELING. Biophysical Reviews and Letters 4:17.
15. Keskin, O., S. R. Durell, I. Bahar, R. L. Jernigan, and D. G. Covell. 2002. Relating molecular flexibility to function: a case study of tubulin. Biophys J 83:663-680.
16. Gebremichael, Y., J. W. Chu, and G. A. Voth. 2008. Intrinsic bending and structural rearrangement of tubulin dimer: molecular dynamics simulations and coarse-grained analysis. Biophys J 95:2487-2499.
17. Mitra, A., and D. Sept. 2008. Taxol allosterically alters the dynamics of the tubulin dimer and increases the flexibility of microtubules. Biophys J 95:3252-3258.
18. Mitra, A., and D. Sept. 2004. Localization of the antimitotic peptide and depsipeptide binding site on beta-tubulin. Biochemistry 43:13955-13962.
19. Mitra, A., and D. Sept. 2006. Binding and interaction of dinitroanilines with apicomplexan and kinetoplastid alpha-tubulin. J Med Chem 49:5226-5231.
20. Leach, A. 2001. Molecular Modelling: Principles and Applications (2nd Edition). {Prentice Hall}.

SUPPORTING MATERIAL 2

Molecular Dynamics set up for curved standard and seam tubulin sheets

Each tubulin sheet (standard and seam sheet) was arranged in a rectangular box of about 15nm × 20nm × 9nm in size, fully solvated by using the single point charge water model (21), and neutralized by sodium ions. Each tubulin sheet consisted of about 53,000 atoms. The total system included about 300,000 atoms.

For both standard tubulin sheet and the seam tubulin sheet models, energy minimization of the system (tubulin-sheet in water) was performed by following a steepest descent optimization scheme (200 steps) for a fast detection of the approximate local minimum energy configuration.

Cutoff distance for non-bonded terms was set up to 1.2 nm. Particle Mesh Ewalds has been used for treating the long-range interactions (with a short range cutoff distance of 1.2 nm) while for short-range interactions a switch function between 1 and 1.1 nm has been used.

A first MD simulation was carried out to heat the system from 0 to 300 K over a period of 100 ps. The temperature was controlled using the weak coupling scheme (22-23) with coupling constant equal to 0.1 ps. During the heating simulation the position of each C_α-atom was restrained by means of a harmonic potential in order to avoid large conformational unfolding of the backbone due to the imposed fast temperature change (2-3).

Equilibration MD simulations were run for 10 ns at 300K in the NVT ensemble. By associating a virtual site approach to the LINCS constraint solver (selecting all-bonds constraint) (24), a timestep of 4 fs was used. In a virtual site approach the bond-angle vibrations involving hydrogen atoms are removed and the masses are properly modified increasing the moment of inertia of the water molecules, the hydroxyl, the sulfhydryl, and the amine groups, without affecting the equilibrium properties of the system and its dynamical properties (25).

During the MD equilibration a constraint was applied to the centre of mass of each monomer surrounding the central tubulin dimer. All the simulations were carried out by using the computational code GROMACS, version 4 (23, 25) , along with the G53a6 GROMOS forcefield (26).

The stabilization of the protein structure in terms of temperature and energy oscillations for both the standard and seam tubulin-sheets was obtained with MD equilibration runs lasting 10 ns each. During these MD simulations, the central tubulin dimer was free to move and rearranged its conformation while interacting with the outer surface of the surrounding monomers Surrounding monomers had their center of mass constrained to maintain the correct position as in the MT B lattice structure, which has been demonstrated to be a configuration in an energetic minimum (27).

References

1. Nogales, E., S. G. Wolf, and K. H. Downing. 1998. Structure of the alpha beta tubulin dimer by electron crystallography. Nature 391:199-203.
2. Enemark, S., M. A. Deriu, M. Soncini, and A. Redaelli. 2008. Mechanical model of the tubulin dimer based on molecular dynamics simulations. J Biomech Eng 130:041008.
3. Deriu, M., S. Enemark, M. Soncini, F. Montevecchi, and A. Redaelli. 2007. Tubulin: from atomistic structure to supramolecular mechanical properties. Journal of Materials Science 42:8864-8872.
4. Lowe, J., H. Li, K. H. Downing, and E. Nogales. 2001. Refined structure of alpha beta-tubulin at 3.5 A resolution. J Mol Biol 313:1045-1057.
5. Downing, K. H., and E. Nogales. 1999. Crystallographic structure of tubulin: implications for dynamics and drug binding. Cell Struct Funct 24:269-275.

6. Downing, K. H., and E. Nogales. 1998. Tubulin structure: insights into microtubule properties and functions. Curr Opin Struct Biol 8:785-791.
7. Downing, K. H., and E. Nogales. 1998. New insights into microtubule structure and function from the atomic model of tubulin. Eur Biophys J 27:431-436.
8. Downing, K. H., and E. Nogales. 1998. Tubulin and microtubule structure. Curr Opin Cell Biol 10:16-22.
9. Li, H., D. J. DeRosier, W. V. Nicholson, E. Nogales, and K. H. Downing. 2002. Microtubule Structure at 8 Å Resolution. Structure 10:1317-1328.
10. Chretien, D., and R. H. Wade. 1991. New data on the microtubule surface lattice. Biol Cell 71:161-174.
11. Fiser, A., and A. Sali. 2003. ModLoop: automated modeling of loops in protein structures. Bioinformatics 19:2500-2501.
12. Sali, A., L. Potterton, F. Yuan, H. van Vlijmen, and M. Karplus. 1995. Evaluation of comparative protein modeling by MODELLER. Proteins 23:318-326.
13. Pearson, W. R. 1990. Rapid and sensitive sequence comparison with FASTP and FASTA. Methods Enzymol 183:63-98.
14. Soncini, M., E. Votta, I. Aprodu, S. Enemark, A. Redaelli, M. A. Deriu, and F. M. Montevecchi. 2009. MICROTUBULE-KINESIN MECHANICS BY MOLECULAR MODELING. Biophysical Reviews and Letters 4:17.
15. Keskin, O., S. R. Durell, I. Bahar, R. L. Jernigan, and D. G. Covell. 2002. Relating molecular flexibility to function: a case study of tubulin. Biophys J 83:663-680.
16. Gebremichael, Y., J. W. Chu, and G. A. Voth. 2008. Intrinsic bending and structural rearrangement of tubulin dimer: molecular dynamics simulations and coarse-grained analysis. Biophys J 95:2487-2499.
17. Mitra, A., and D. Sept. 2008. Taxol allosterically alters the dynamics of the tubulin dimer and increases the flexibility of microtubules. Biophys J 95:3252-3258.
18. Mitra, A., and D. Sept. 2004. Localization of the antimitotic peptide and depsipeptide binding site on beta-tubulin. Biochemistry 43:13955-13962.
19. Mitra, A., and D. Sept. 2006. Binding and interaction of dinitroanilines with apicomplexan and kinetoplastid alpha-tubulin. J Med Chem 49:5226-5231.
20. Leach, A. 2001. Molecular Modelling: Principles and Applications (2nd Edition). {Prentice Hall}.
21. Berendsen, H. J. C., J. P. M. Postma, W. F. Vangunsteren, A. Dinola, and J. R. Haak. 1984. Molecular-Dynamics with Coupling to an External Bath. J Chem Phys 81:3684-3690.
22. Berendsen, H. J. C., J. P. M. Postma, W. F. van Gunsteren, A. Dinola, and J. R. Haak. 1984. Molecular dynamics with coupling to an external bath. The Journal of Chemical Physics 81:3684-3690.
23. Hess, B., C. Kutzner, D. van der Spoel, and E. Lindahl. 2008. GROMACS 4: Algorithms for Highly Efficient, Load-Balanced, and Scalable Molecular Simulation. Journal of Chemical Theory and Computation 4:435-447.
24. Berk Hess, Henk Bekker, Herman J. C. Berendsen, and Johannes G. E. M. Fraaije. 1997. LINCS: A linear constraint solver for molecular simulations. Journal of Computational Chemistry 18:1463-1472.
25. Van Der Spoel, D., E. Lindahl, B. Hess, G. Groenhof, A. E. Mark, and H. J. Berendsen. 2005. GROMACS: fast, flexible, and free. J Comput Chem 26:1701-1718.
26. Oostenbrink, C., A. Villa, A. E. Mark, and W. F. Van Gunsteren. 2004. A biomolecular force field based on the free enthalpy of hydration and solvation: The GROMOS force-field parameter sets 53A5 and 53A6. Journal of Computational Chemistry 25:1656-1676.
27. Sept, D., N. A. Baker, and J. A. McCammon. 2003. The physical basis of microtubule structure and stability. Protein Sci 12:2257-2261.
28. Marques, O., and Y. H. Sanejouand. 1995. Hinge-bending motion in citrate synthase arising from normal mode calculations. Proteins 23:557-560.
29. Tama, F., F. X. Gadea, O. Marques, and Y. H. Sanejouand. 2000. Building-block approach for determining low-frequency normal modes of macromolecules. Proteins 41:1-7.

30. Philippe Durand, Georges Trinquier, and Yves-Henri Sanejouand. 1994. A new approach for determining low-frequency normal modes in macromolecules. Biopolymers 34:759-771.
31. Tama, F., and C. L. Brooks, 3rd. 2005. Diversity and identity of mechanical properties of icosahedral viral capsids studied with elastic network normal mode analysis. J Mol Biol 345:299-314.
32. Tama, F., and Y.-H. Sanejouand. 2001. Conformational change of proteins arising from normal mode calculations. Protein Eng. 14:1-6.
33. Li, G., and Q. Cui. 2002. A coarse-grained normal mode approach for macromolecules: an efficient implementation and application to Ca(2+)-ATPase. Biophys J 83:2457-2474.
34. Flynn, T. C., and J. Ma. 2004. Theoretical analysis of twist/bend ratio and mechanical moduli of bacterial flagellar hook and filament. Biophys J 86:3204-3210.
35. Park, J., B. Kahng, R. D. Kamm, and W. Hwang. 2006. Atomistic simulation approach to a continuum description of self-assembled beta-sheet filaments. Biophys J 90:2510-2524.
36. Adamovic, I., S. M. Mijailovich, and M. Karplus. 2008. The elastic properties of the structurally characterized myosin II S2 subdomain: a molecular dynamics and normal mode analysis. Biophys J 94:3779-3789.
37. Meirovitch, L. 1967. Analytical methods in vibrations. Macmillan, New York.
38. Meirovitch, L. 1970. Methods of analytical dynamics. McGraw-Hill, New York.
39. Meirovitch, L. 2003. Methods of analytical dynamics. Dover, Mineola, N.Y.

SUPPORTING MATERIAL 3

Rotation Translation Block approach

There are a number of bottlenecks associated to the diagonalization of the Hessian matrix **H**, in particular, when the system becomes very big (more than ten thousands atoms).
First of all, the storage of **H** formally scales as $(3N)^2/2$, where *N* is the number of atoms in the system. Usually **H** quickly exceeds the memory of a typical workstation requiring more than 4, 8 and sometimes more than 16 GB of RAM.
Second, the diagonalization of **H** scales as N^3 with standard algorithms. If just a small number of eigenvalues (and corresponding eigenvectors) are needed, iterative approaches such as BLZPACK, based on the block Lanczos algorithm could be used (28-29).
Another strategy for performing normal mode analysis (NMA) for large molecules is to use a coarse-grained approach (coarser than just using the C_α-atoms). This is particularly useful when only the low frequencies (e.g., lower than 10^{-1} cm) are of interest since the low-frequency motions are typically delocalized throughout the system and involve mainly collective movements of residues.
Promising approaches for performing effective NMA are the Block Normal Mode approach or Rotation Translation Block (RTB) method (29-32).
In the Rotation Translation Block (RTB) approach the molecular system is divided in n_b rigid blocks; each block is made of a certain number of residues (each represented by C_α-atoms) considered as a rigid body, and for this reason each block must contain at least three atoms. The deformation of the whole system is given by rotation-translation movements of the rigid blocks (29). In particular, **H**, is expressed in a basis, $\mathbf{H_b}$, defined by rotations and translations of the n_b rigid blocks (29-30).

1 $$\mathbf{H}_b = \mathbf{P}^T \mathbf{H} \mathbf{P}$$

where **P** is an orthogonal $3N$ x $6n_b$ matrix built with the vector associated to the local rotations/translations of each block. Approximate low-frequency normal modes are calculated by diagonalizing through standard methods, $\mathbf{H_b}$, which is a reduced matrix of size $6n_b$ x $6n_b$, instead of the entire matrix **H** of size $3N$ x $3N$, where *N* is the number of C_α-atoms in the system (29).
The corresponding atomic displacements of all C_α-atoms is given by:

2 $$\mathbf{A}_p = \mathbf{P}\mathbf{A}_b$$

where $\mathbf{A}_b$ is the matrix of the eigenvectors of $\mathbf{H_b}$.
The eigenvectors can be expanded back to the atomic space using the transpose of the projector **P**. It has been demonstrated (29, 33) that the eigenvalues and the eigenvectors calculated by using RTB closely approximate those obtained by diagonalizing the atomic **H**.
Then, structural and dynamic properties as root mean square fluctuations (RMSF) can be evaluated based on the eigenvalues and eigenvectors.

References

1. Marques, O., and Y. H. Sanejouand. 1995. Hinge-bending motion in citrate synthase arising from normal mode calculations. Proteins 23:557-560.
2. Tama, F., F. X. Gadea, O. Marques, and Y. H. Sanejouand. 2000. Building-block approach for determining low-frequency normal modes of macromolecules. Proteins 41:1-7.
3. Philippe Durand, Georges Trinquier, and Yves-Henri Sanejouand. 1994. A new approach for determining low-frequency normal modes in macromolecules. Biopolymers 34:759-771.
4. Tama, F., and C. L. Brooks, 3rd. 2005. Diversity and identity of mechanical properties of icosahedral viral capsids studied with elastic network normal mode analysis. J Mol Biol 345:299-314.
5. Tama, F., and Y.-H. Sanejouand. 2001. Conformational change of proteins arising from normal mode calculations. Protein Eng. 14:1-6.
6. Li, G., and Q. Cui. 2002. A coarse-grained normal mode approach for macromolecules: an efficient implementation and application to Ca(2+)-ATPase. Biophys J 83:2457-2474.

SUPPORTING MATERIAL 4

Estimating Protein Mechanical Properties from NMA

The vibrational normal modes of a filament (such as a MT) can be related to its mechanical stiffness (34-38).
Under the assumption that the filament is a linear elastic material, its compliance can be characterized by stiffness values: stiffness in bending, also called flexural rigidity k_f, or stiffness in elongation k_s, or stiffness in torsion k_t, depending on the deformation status.
For small deformations the displacement components, as function of the axial coordinate (e.g., z) and time t satisfy the following wave equations for bending displacement $u_f(z,t)$, stretching displacement $u_s(z,t)$, and torsion displacement $u_\vartheta(z,t)$:

3 $$\rho \frac{\partial^2 u_f(z,t)}{\partial t^2} = -k_f \frac{\partial^4 u_f(z,t)}{\partial z^4}$$

4 $$\rho \frac{\partial^2 u_s(z,t)}{\partial t^2} = -k_s \frac{\partial^2 u_s(z,t)}{\partial z^2}$$

5 $$\rho_v I \frac{\partial^2 u_\theta(z,t)}{\partial t^2} = -k_t \frac{\partial^2 u_\theta(z,t)}{\partial z^2}$$

Where ρ is the mass per length unit of the filament roughly equal to 2 10^{-15} Kg/m (for the MT considered as a hollow cylinder) and ρ_v is the mass per volume unit of the filament roughly equal to 15 Kg/m^3 for a 13:3 MT.

The general solution of eq. 3,4 and 5 can be expressed as a linear combination of hyperbolic sinusoidal waves:

6 $$u_f(z,t) \approx \begin{pmatrix} \cos(w_n z) \\ \sin(w_n z) \\ \cosh(w_n z) \\ \sinh(w_n z) \end{pmatrix} e^{-i\omega_n t}$$

7 $$u_s(z,t) \approx \begin{pmatrix} \sin(w_n z) \\ \cos(w_n z) \end{pmatrix} e^{-i\omega_n t}$$

8 $$u_\vartheta(z,t) \approx \begin{pmatrix} \sin(w_n z) \\ \cos(w_n z) \end{pmatrix} e^{-i\omega_n t}$$

The last two systems of equations can be used to find the dispersion relation between wave number w_n, and angular frequency ω_n (1/s) , resulting:

9 $$\rho\omega_n^{\,2} = k_f w_n^{\,4}$$

10 $$\rho\omega_n^{\,2} = k_s w_n^{\,2}$$

11 $$\rho_v I\omega_n^{\,2} = k_t w_n^{\,2}$$

where I is the moment of inertia of the cross-sectional area with respect to the corresponding axis of deflection, which is about 1 10^{-32} m^4 for a 13:3 MT. Depending on the boundary conditions, there are specific linear combinations of the general solution (eq. 3,4,5). In particular, in the case of NMA the filament is not clamped, so the correspondent boundary conditions, both in bending or stretching are $u'_{f,s}(0)=0$ and $u''_{f,s}(L_{MT})=0$, where L_{MT} is the filament length.
In the case of bending modes the corresponding solution of a free vibrating filament with length L_{MT} is given by:

12
$$u_f(z,t) = \sum_n a_n \left\{ -\left[\cos(w_n z) + \cosh(w_n z)\right] - \left(\frac{\cos(w_n z) - \cosh(w_n z)}{\sin(w_n z) - \sinh(w_n z)} \right) \left[\sin(w_n z) + \sinh(w_n z)\right] \right\} e^{-i\omega_n t}$$

where the wave number w_n is given by the relation:

13 $$\cos(w_n L_{MT}) + \cosh(w_n L_{MT}) = 1.$$

In the absence of viscous drag, the amplitude a_n of the n^{th} mode is, in principle, determined by the initial conformation of the filament.
In the case of stretching or torsion modes the corresponding solution is given by:

14 $$u_s(z,t) = \sum_n a_n \cos(w_n z)\ e^{-i\omega_n t},$$

where the wave number w_n for the n^{th} mode is given simply by the relation:

15 $$w_n = \frac{n\pi}{L_{MT}}.$$

Once the normal modes and the related frequencies are calculated, it is possible to estimate the mechanical proprieties applying the linear elastic beam theory (37-39).

A linear elastic beam is characterized by a constant stiffness value when deformations as bending k_f, stretching k_s, or torsion k_t are applied. The constant stiffness is directly related to the eigenvalue of the correspondent mode in both cases.
The bending modulus Y_f, can be calculated as:

16 $$Y_f = \frac{k_f}{I}$$

Under the assumption of isotropic and homogenous material the bending modulus is equal to the Young's modulus. Alternatively, the stretching modulus Y_x, i.e. the Young's modulus, can be calculated directly by the stretching modes, as:

17 $$Y_x = \frac{k_s}{A} L_{MT}$$

where k_s is the stretching stiffness, A is the cross-sectional area of the filament (which in the case of 13:3 MT is about to 1.8 10^{-16} m^2). The shear modulus can be directly obtained by the torsion stiffness k_t, as:

18 $$G = \frac{k_t}{J}$$

where J is the polar moment of inertia roughly equal to 2 10^{-32} m^4, which is twice the moment of inertia of the cross-sectional area I.
The persistence length l_p, is related to the bending stiffness k_f, the Boltzmann constant k_B, and the temperature T, through:

19 $$l_p = \frac{k_f}{k_B T}$$

References

1. Flynn, T. C., and J. Ma. 2004. Theoretical analysis of twist/bend ratio and mechanical moduli of bacterial flagellar hook and filament. Biophys J 86:3204-3210.
2. Park, J., B. Kahng, R. D. Kamm, and W. Hwang. 2006. Atomistic simulation approach to a continuum description of self-assembled beta-sheet filaments. Biophys J 90:2510-2524.
3. Adamovic, I., S. M. Mijailovich, and M. Karplus. 2008. The elastic properties of the structurally characterized myosin II S2 subdomain: a molecular dynamics and normal mode analysis. Biophys J 94:3779-3789.
4. Meirovitch, L. 1967. Analytical methods in vibrations. Macmillan, New York,.
5. Meirovitch, L. 1970. Methods of analytical dynamics. McGraw-Hill, New York,.
6. Meirovitch, L. 2003. Methods of analytical dynamics. Dover, Mineola, N.Y.